Faculty Scholarship

1995

Instabilities in propagating reaction-diffusion fronts of the iodate-arsenous acid reaction

Dezső Horváth

Kenneth Showalter

Follow this and additional works at: https://researchrepository.wvu.edu/faculty_publications

Instabilities in propagating reaction-diffusion fronts of the iodate-arsenous acid reaction

Dezső Horváth and Kenneth Showalter[a)]

Department of Chemistry, West Virginia University, Morgantown, West Virginia 26506

Instabilities in propagating fronts of the iodate-arsenous acid reaction are predicted by an empirical rate-law model. The planar front loses stability when the ratio of the reactant diffusivity to the autocatalyst diffusivity exceeds a critical value. The relative diffusivities can be altered by introducing a reagent that reacts specifically with the autocatalyst to form an immobile complex. Experiments were carried out using a convection-free gelled medium, loaded with reaction mixture containing complexing agent at different concentrations. Instabilities were found above a critical concentration, with the appearance of cellular fronts much like those predicted by the empirical rate-law model. © *1995 American Institute of Physics.*

I. INTRODUCTION

Instabilities leading to spontaneous pattern formation in reaction-diffusion systems arise from the spatial decoupling of key species, known as the activator and inhibitor species, by some form of transport.[1] The activator is typically an autocatalytic species and the inhibitor a species that acts to inhibit autocatalysis. The inhibitor may be produced by the autocatalytic process or it may be simply a stoichiometrically deficient reactant of that process. In pattern formation developing from a Turing instability, the spatial decoupling arises from a difference in the activator and inhibitor diffusivities.[2] A differential flow of these species may also give rise to pattern formation.[3] A similar spatial decoupling occurs in the thermodiffusive instability of premixed flames, where the heat of reaction plays the role of the activator and a stoichiometrically deficient fuel acts as the inhibitor.[4] In systems with the Lewis number exceeding a critical value, where the molecular diffusivity is higher than the thermal diffusivity, the planar flame front loses its stability with the appearance of cellular structures.[5] Recent theoretical studies have shown that a similar instability may occur in an isothermal reaction-diffusion front when the diffusivity of the autocatalyst is sufficiently lower than that of the stoichiometrically deficient reactant.[6] We focus in this paper on such front instabilities in an experimental system, the iodate-arsenous acid reaction.

Propagating fronts in the iodate-arsenous acid reaction arise from the diffusive spread of autocatalytically generated iodide into surrounding regions of solution containing fresh reactants. The stability of the planar front depends on the relative diffusivities of iodide and the reactant iodate, which is stoichiometrically limiting in the excess arsenous acid system considered here. A disturbance in the front will either grow or decay depending on whether the diffusion of iodate or iodide is dominant.[6,7] The diffusion of the autocatalyst tends to cause the decay of any disturbance, thereby stabilizing the planar front. This can be seen by considering how the autocatalyst diffuses ahead at a disturbance that is either convex or concave (in the direction of the front propagation). At a convex disturbance, the diffusive dispersion of iodide is enhanced and the advancement of the wave is consequently retarded. The opposite is true at a concave disturbance, where the iodide is diffusively focused. Here the wave advancement is enhanced. Hence, the diffusion of the autocatalyst tends to "raise the valleys and lower the peaks," smoothing out the disturbances. The diffusion of the reactant iodate, on the other hand, tends to be destabilizing. At a convex disturbance, the diffusion of iodate into the front is focused and the advancement of the wave is enhanced; at a concave disturbance, the advancement of the wave is retarded due to the diffusive dispersion of the reactant. The diffusion of iodate tends to "lower the valleys and raise the peaks," with the growth of disturbances.

There exists a critical ratio of the reactant and autocatalyst diffusion coefficients above which the planar front loses its stability and cellular patterns develop.[6] For pure cubic autocatalysis, a value of 2.9 was numerically determined for the critical ratio. Following Sivashinsky,[5] an analytical analysis was also carried out by assuming reaction occurs in an infinitely narrow zone in the front. This treatment yielded a critical ratio of 2.0 for the onset of instability. In studies of quadratic and cubic mixed-order fronts, we found the cubic nonlinearity to be a prerequisite for the onset of instability.

The iodate-arsenous acid reaction was chosen for our experimental study of front instabilities because it is governed by a quadratic and cubic mixed-order rate law analogous to that in our theoretical study. The propagating front of the reaction can be described nearly quantitatively by a model based on the empirical rate law.[8,9] In this study, we present a modification of the model that accounts for the front instabilities found in our experiments.

Propagating iodate-arsenous acid fronts were studied in cross-linked gels (as a convection-free medium) loaded with α-cyclodextrin, a species that forms an immobile complex with the autocatalyst iodide. The ratio of the effective diffusion coefficients can be varied by adjusting the concentration of the complexing agent, and it can be raised above the critical value. In Sec. II we present results from a numerical study of the modified empirical rate-law model. Our experimental study of front instabilities is described in Sec. III. We conclude in Sec. IV with an analysis of how the front propagation is affected by the complex formation. We also com-


[a)]Author to whom correspondence should be addressed.

pare the instabilities in isothermal reaction-diffusion fronts with those in nonisothermal flame fronts.

## II. MODELING STUDY

A. Empirical rate-law model

The iodate oxidation of arsenous acid can be described in terms of two component processes,[10] each with a long history in chemical kinetics. Process (1), the iodate oxidation of iodide, was first studied by Dushman[11] in 1904:

$$5I^- + IO_3^- + 6H^+ \rightarrow 3I_2 + 3H_2O. \tag{1}$$
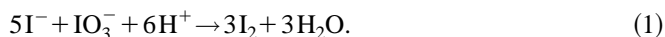
The reaction is effectively irreversible at the acidities of our experiments, with the conversion of iodate and iodide to molecular iodine virtually quantitative. Process (2), the iodine oxidation of arsenous acid, was first studied by Roebuck[12] in 1902:

$$I_2 + H_3AsO_3 + H_2O \rightleftharpoons 2I^- + H_3AsO_4 + 2H^+. \tag{2}$$

This reaction is reversible; however, the equilibrium lies far to the right for the hydrogen ion concentrations of our experiments. When the reaction is carried out with arsenous acid in stoichiometric excess, the net stoichiometry is given by (1)+3(2):

$$3H_3AsO_3 + IO_3^- = 3H_3AsO_4 + I^-. \tag{3}$$
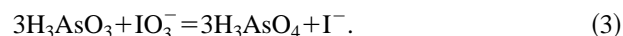
Under these conditions, the rate determining step is the Dushman reaction, for which a two-term rate law has been established:[13]

$$r([IO_3^-],[I^-]) \equiv \frac{d[I^-]}{dt} = (k_a + k_b[I^-])[I^-][IO_3^-][H^+]^2, \tag{4}$$

where $k_a = 4.5 \times 10^3$ M^{-3} s^{-1} and $k_b = 4.5 \times 10^8$ M^{-4} s^{-1}.[13,14]

Because I$^-$ is a product of net reaction (3) and the rate law for the Dushman reaction is first and second order in I$^-$, the overall reaction is autocatalytic in iodide. The reaction is also autocatalytic in hydrogen ion; however, we focus on experiments carried out in buffered solutions where [H$^+$] is essentially constant.

For an effectively two-dimensional thin film of solution (or gel), the reaction-diffusion system is described by the partial differential equations

$$\frac{\partial[IO_3^-]}{\partial t} = D_{IO_3^-}\nabla^2[IO_3^-] - r([IO_3^-],[I^-]), \tag{5}$$

$$\frac{\partial[I^-]}{\partial t} = D_{I^-}\nabla^2[I^-] + r([IO_3^-],[I^-]), \tag{6}$$

where ∇^2 is the two-dimensional (2D) Laplacian operator. Both diffusion coefficients are taken as $D = 2.0 \times 10^{-5}$ cm^2 s^{-1}, a typical value for solvated ions in aqueous solution. We use this value for modeling our experiments carried out in acrylamide gels, since the diffusivities of iodide and iodate in such gels have not been measured.

A necessary condition for the onset of instability is for the diffusivity of the autocatalyst to be sufficiently lower than that of the reactant. An appropriate reagent for lowering the effective diffusivity of iodide is α-cyclodextrin, which is

TABLE I. Reagent concentrations.

	Reactant mixture	Product mixture
[IO$_3^-$] (M)	0.0048	
[I$^-$] (M)	<10^{-7} [a]	0.0048
[As(III)] (M)	0.016	0.016
[SO$_4^{2-}$] (M)	0.32	0.32
[HSO$_4^-$] (M)	0.048	0.048
[Ag$^+$] (M)	6.5 × 10^{-5}	
pH	2.35	2.35

[a]Maximum amount from impurities.

sufficiently bulky that its diffusivity is significantly reduced in a highly cross-linked gel. (Even in aqueous solution the diffusion coefficient of β-cyclodextrin,[15] which is very similar to α-cyclodextrin, is 3.3×10^{-6} cm^2 s^{-1}, almost an order of magnitude lower than the diffusion coefficients typical of small ions and molecules.) Iodide and α-cyclodextrin form a complex according to the equilibrium

$$I^- + \text{cyclodextrin} \underset{}{\overset{K_{CD}}{\rightleftharpoons}} \text{cyclodextrin-}I^-, \tag{7}$$

where $K_{CD} = 13$ M^{-1}.[16] Relaxation measurements have shown this equilibrium to be rapid.[17]

We now consider the effect of the complex formation on the diffusivity of iodide. We follow the treatment proposed by Lengyel and Epstein[18] for explaining the reduced diffusivity of triiodide ion in the CIMA (chlorite-iodide-malonic acid) reaction, which gives rise to the Turing instability in that system. Their treatment is based on the reversible formation of the starch-triiodide complex, in which the forward and reverse reactions are assumed to be rapid. We first rewrite Eq. (6) in terms of the total amount of iodide ion present in the system, [I$^-$]$_t$ = [I$^-$]+[cyclodextrin-I$^-$]:

$$\frac{\partial[I^-]_t}{\partial t} = D_{I^-}\nabla^2[I^-] + r([IO_3^-],[I^-]), \tag{8}$$

where we assume that the diffusion of the cyclodextrin-iodide complex is negligible in the cross-linked polymeric structure of the gel. When the complexing agent is in large excess, the concentration of the total iodide present in the system can be expressed as a function of free iodide concentration according to equilibrium (7),

$$[I^-]_t = (K_{CD}[\text{cyclodextrin}]_0 + 1)[I^-] \equiv \sigma[I^-], \tag{9}$$

where [cyclodextrin]$_0$ is the total concentration of the complexing agent. A partial differential equation for free iodide can be obtained by differentiating Eq. (9) with respect to time and substituting the result into Eq. (8):

$$\frac{\partial[I^-]}{\partial t} = \frac{D_{I^-}}{\sigma}\nabla^2[I^-] + \frac{r([IO_3^-],[I^-])}{\sigma}. \tag{10}$$

Equation (6) must be replaced by Eq. (10) to model reaction mixtures containing cyclodextrin in large excess. Because cyclodextrin does not bind with iodate ion, Eq. (5) remains unchanged. The complex formation lowers the apparent diffusion coefficient of free iodide, since σ is always greater than unity.
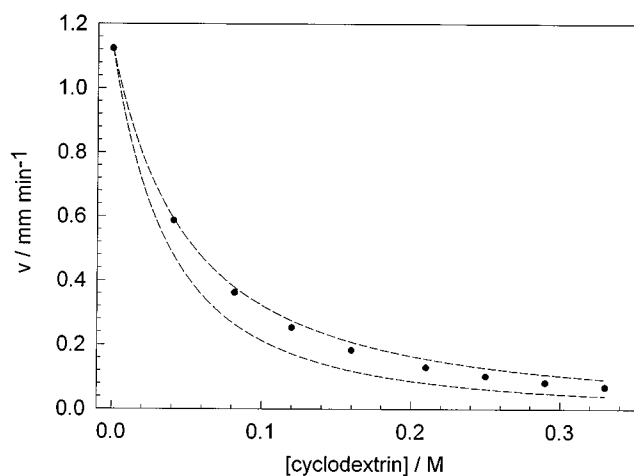
FIG. 1. Velocity of fronts as a function of α-cyclodextrin concentration predicted by empirical rate-law model. Equations (5) and (10) were numerically integrated using the rate constants $k_a = 4.5 \times 10^3$ $M^{-3} s^{-1}$ and $k_b = 4.5 \times 10^8$ $M^{-4} s^{-1}$, equilibrium constant $K_{CD} = 13$ M^{-1}, and diffusion coefficients $D = 2.0 \times 10^{-5}$ $cm^2 s^{-1}$. The integration was carried out on a 101×121 grid with 0.0625 cm grid spacing and a time step of 0.25 s. The reactant concentrations are given in Table I. Dashed curves represent upper and lower bounds for the velocity dependence on $[cyclodextrin]_0$ as discussed in Sec. IV.
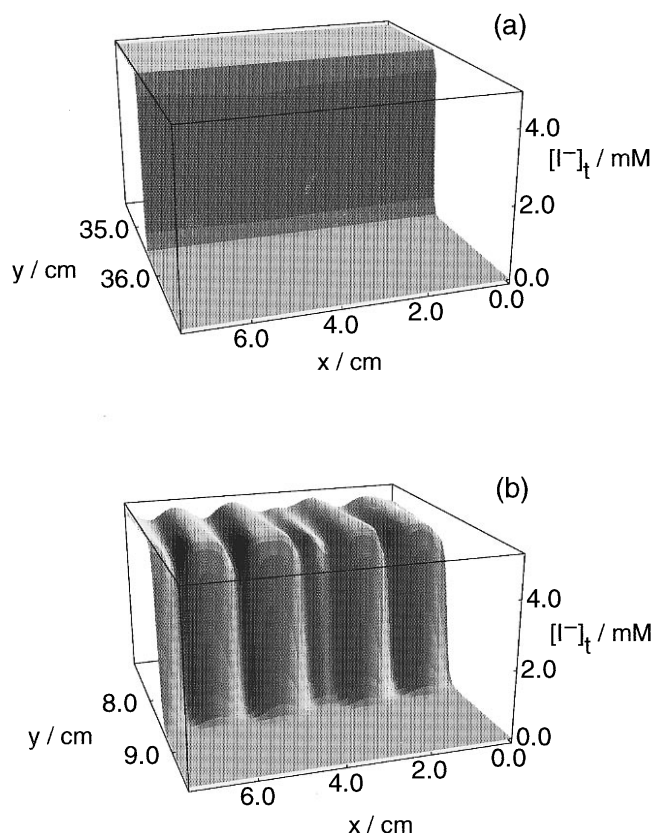

FIG. 2. Concentration profiles of fronts with cyclodextrin concentrations (a) below and (b) above the critical value for the onset of instability. (a) Front propagating in y direction at $t=10$ h into reactant zone with $[cyclodextrin]_0 = 0.04$ M; (b) front at $t=21$ h with $[cyclodextrin]_0 = 0.33$ M.

The numerical integration of the two-variable model given by Eqs. (5) and (10) was carried out by approximating the Laplacian with a standard nine-point formula on a 101 $\times 121$ grid with 0.0625 cm grid spacing and no-flux boundary conditions. The ODEs were solved by applying an explicit Euler method with a time step of 0.25 s. The grid spacing and time step were varied to determine appropriate values for the integration, where the front behavior does not change with successively smaller values. The initial conditions were chosen to reflect the experimental configuration. The grid was divided into two regions: one corresponding to the reactant mixture ahead of the front, containing only iodate and arsenous acid; the other corresponding to the product mixture behind the front, containing only iodide and arsenous and arsenic acids. The front initially formed along the boundary and immediately began to propagate into the reactant zone. The reactant concentrations used in the modeling study correspond to those used in the experiments (see Table I).

B. Modeling results

Figure 1 shows velocities of front propagation calculated from Eqs. (5) and (10) for a range of cyclodextrin concentrations. The velocity of 1.12 mm min^{-1} at $[cyclodextrin]_0 = 0$ is in good agreement with previously measured velocities of waves in thin layers of iodate-arsenous acid solutions.[8] It agrees reasonably well with the value of 1.25 mm min^{-1} predicted from the analytical solution of Eqs. (5) and (6) for the case of equal diffusion coefficients.[8,9] As the cyclodextrin concentration is increased, a greater fraction of the iodide is bound in the immobile complex and less free iodide is available to diffuse

ahead in the propagating front. The propagation velocity therefore decreases. The velocity is also lowered by the decrease in effective rate, which is inversely proportional to the value of σ according to Eq. (10). An analysis of the velocity decrease with increasing $[cyclodextrin]_0$ is presented in Sec. IV.

The initial conditions for the calculations included random perturbations in the interface between the reactant and product zones, where the product zone was either advanced by one pixel or left unchanged at each grid point along the boundary. In calculations with $[cyclodextrin]_0 \leq 0.12$ M, the imposed perturbations rapidly decay with the front retaining its planar character. A typical planar front is shown in Fig. 2(a), in which $[cyclodextrin]_0 = 0.04$ M. In calculations with $[cyclodextrin]_0 \geq 0.16$ M, however, the planar front loses its stability to yield a structured wave profile like that shown in Fig. 2(b), where $[cyclodextrin]_0 = 0.33$ M. The range of $[cyclodextrin]_0$ between 0.12 and 0.16 M for the onset of instability corresponds to our ability to discern the nonplanar behavior in the experimental measurements, as explained below. This cyclodextrin concentration range corresponds to σ values between 2.6 and 3.1, in good agreement with $\sigma = 2.9$ obtained from our numerical analysis of cubic autocatalysis fronts.[6]

The experimental measurements of fronts in iodate-arsenous acid solutions containing cyclodextrin relied on the detection of iodine by absorbance of light at 400 nm. In
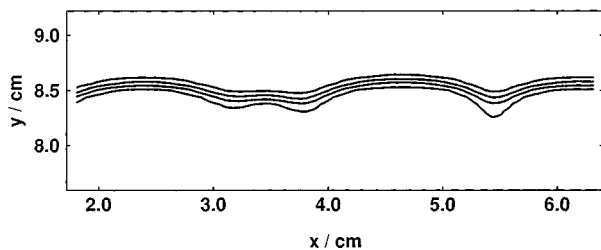
FIG. 3. Contour lines at $[I^-]_t = 1.0, 2.0, 3.0,$ and 4.0 mM of the front in Fig. 2(b) for the region $2.0 < x < 6.0$. Front is propagating in the positive y direction.

reaction mixtures containing excess arsenous acid, I_2 appears in low concentrations as an intermediate species. Its transient appearance occurs near the midpoint of the iodide concentration rise, forming a narrow band along the front.[8] In order to provide a comparison of the modeling results with the experimental measurements, we represent the front shown in Fig. 2(b) by plotting contour lines that span the steepest part of the iodide concentration rise, as shown in Fig. 3. The valleys between the cellular structures in the 3D profile appear as shallow cusps in the contour lines. The curvature is greater where the cells are joined at the cusps than along the foremost sections of the cells.

The front profile in Figs. 2(b) and 3 represents a snapshot of a continually changing structure. The evolution of this structure can be monitored by following the positions of the valleys between the cellular structures. This is carried out by determining the minima in one of the contour lines, and plotting the positions of these minima in the x and y directions at regular time intervals, as shown in Fig. 4. As the front propagates ahead into fresh reactants, the minima propagate along the front as transverse waves. The waves disappear on collision with the no-flux boundaries, and new waves spontaneously appear along the front in regions where the distance between two adjacent waves is relatively large. Waves colliding with one another form a single wave. The velocities of the transverse waves are much lower than the

FIG. 5. Initial front evolution calculated from a symmetrical perturbation with $[cyclodextrin]_0 = 0.33$ M. (a) Behavior at $t = 23$ min following initiation at interface between product and reactant zones. (b) Development of front at $t = 343$ min after initiation with the appearance of a cusp separating two symmetrical cells.

overall front velocity. Detailed calculations show that even simple two-cell fronts (with a single cusp) display extremely complex oscillatory behavior, including a period-doubling sequence that leads to chaos.[6]

Irregular spatiotemporal behavior is exhibited over the parameter range where measurements of cellular structures were possible in our experimental study. To provide an additional comparison between the model calculations and experimental measurements, we also monitored the formation and evolution of the front structure arising from a single, symmetrical perturbation. Rather than a random pixel-by-pixel displacement of the initial product-reactant interface, the middle third of the interface was advanced by four pixels with respect to the segments on either side, as shown in Fig. 5(a). With these initial conditions, a distinctive two-cell structure initially develops as the front evolves—provided the cyclodextrin concentration is above the critical value. As shown in Fig. 5(b), a minimum occurs in the center of the advanced segment where the two symmetrical cells join. This structure eventually gives way to complex behavior like that shown in Fig. 3; however, we focus on the transient initial wave form in our comparison with the experimental behavior. When the cyclodextrin concentration is below the critical level, the sharp corners of the initial perturbation are diffusively smoothed and no central minimum is exhibited. The rounded, featureless front eventually flattens out to yield a planar front. An example of this behavior, with $[cyclodextrin]_0 = 0.04$ M, is shown in Fig. 6(b). The initial perturbation is shown in Fig. 6(a).
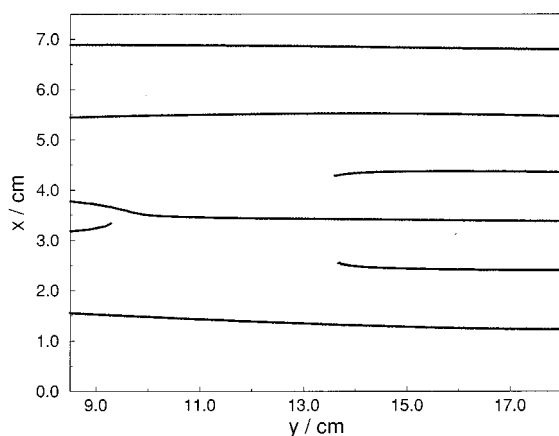

FIG. 4. Evolution of the minima in the $[I^-]_t = 4.0$ mM isoconcentration contour for the front shown in Fig. 2(b). The minima undergo lateral movement as the cellular structure rearranges.
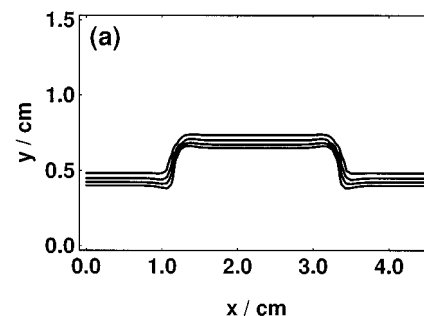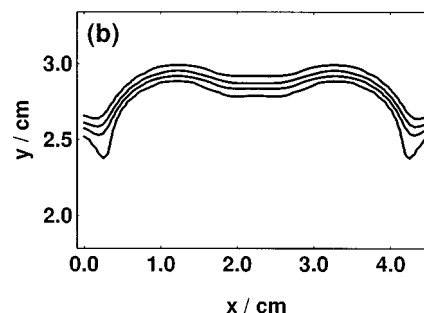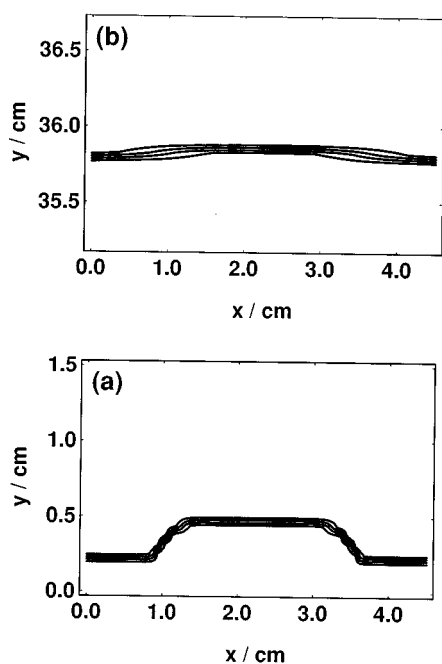
FIG. 6. Initial front evolution calculated from a symmetrical perturbation with $[\text{cyclodextrin}]_0 = 0.04$ M. (a) Behavior at $t = 10$ min following initiation at interface between product and reactant zones. (b) Development of front at $t = 10$ h after initiation showing the diffusive smoothing of the perturbation.
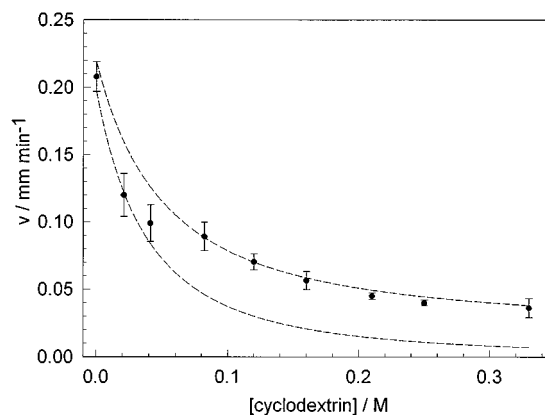

FIG. 7. Measured velocity of front propagation as a function of cyclodextrin concentration. Error bars give standard deviation of velocity measurements from three to five separate experiments. Reactant concentrations are given in Table I. Dashed curves represent upper and lower bounds for the velocity dependence on $[\text{cyclodextrin}]_0$ as discussed in Sec. IV.

III. EXPERIMENTAL STUDY

A. Solutions and experimental procedures

Stock solutions were prepared with reagent grade chemicals and doubly distilled water. The gel was prepared according to the procedure of Noszticzius et al.[19] In 15 ml of water, 3.0 g of acrylamide and 0.60 g of the cross-linker N,N'-methylenebisacrylamide were dissolved. After the addition of 0.3 ml of 30% triethanolamine solution, the solution was degassed and cooled to ~5 °C. A 30 mg quantity of solid ammonium disulfate was dissolved in the solution, which was then injected into a Plexiglas mold designed to produce a rectangular sheet of gel measuring 7.5 cm×15.0 cm×1.0 mm. The polymerization took place within 30 min. The gel was then soaked in distilled water for several hours. Each gel was prepared with α-cyclodextrin added to the mixture of monomer and cross-linker before polymerization.

The cured gel was divided into two parts with a specially shaped blade. The larger part was immersed in a buffered reactant solution containing iodate, arsenous acid and cyclodextrin. The smaller part was immersed in a buffered product solution containing iodide. Both solutions were prepared according to the compositions in Table I, with iodate replaced by an equal amount of iodide in the product solution. (Some experiments were carried out using actual product solutions; however, reactant solutions with iodide replacing iodate were used in most experiments.) The reactant solution was prepared so that the cyclodextrin concentration matched the concentration in the gel. A small amount of silver nitrate was also added to the reactant solution to suppress autoinitiation of wave activity. No silver ion was added to the product

mixture. The two segments of gel were joined smoothly along the cut edge and placed into a Plexiglas jacket thermostated at 25.0 ± 0.2 °C.

The front was visualized by taking advantage of the strong optical absorbance of iodine at the broad band centered at 352 nm. The gel was illuminated from below by light passing through a broad band interference filter with a 400 nm peak transmittance (Oriel, 57520). An integrating sphere (Oriel, 70481) was used to produce homogeneous illumination of the gel. The front was monitored with a video camera (Pulnix, TM-7CN) placed above the reactor. Images were typically acquired at 20 min intervals for up to 40 h and stored digitally using a frame grabber (Matrox, MVP-AT). Three intensity profiles from each image were taken (in the direction of propagation) for the velocity measurements. The front position as a function of time was determined from the gray level minima in the profiles, from which the average velocity was obtained.

B. Experimental results

Measured velocities of fronts propagating in gels loaded with iodate, arsenous acid and cyclodextrin are shown in Fig. 7. The velocity decreases with increasing cyclodextrin concentration, as expected from the modeling results. The magnitudes of the measured values, however, are lower than the values calculated from Eqs. (5) and (10) by about a factor of 5. This discrepancy is due to the high cross linking of the polyacrylamide gel, which was necessary to reduce the mobility of the cyclodextrin-I^- complex. Experiments carried out with low cross linking (1:25 cross-linker N,N'-methylenebisacrylamide to acrylamide) yielded a velocity of 1.00 mm min^{-1} for $[\text{cyclodextrin}]_0 = 0$, in reasonably good agreement with the velocity calculated from Eqs. (5) and (10) for the corresponding conditions. The velocity dropped to 0.197 mm min^{-1} when the cross linking was increased to a level sufficient to immobilize the cyclodextrin-I^- complex (1:5 cross-linker to acrylamide). The homogeneity of the medium was not broken by the high
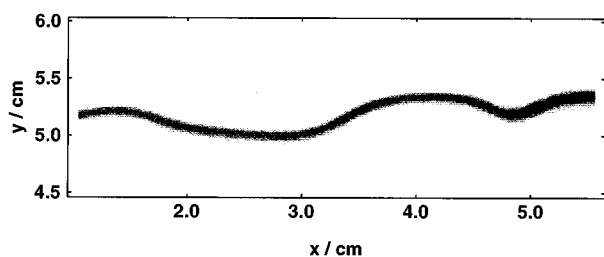
FIG. 8. The middle section of an evolving front at ~24 h after initiation at a planar interface between product and reactant zones. Reactant concentrations are given in Table I with [cylodextrin]$_0$=0.33 M.

cross linking, which may occur in some highly cross-linked polymers,[20] since the fronts in gels containing cyclodextrin below the critical concentration were always found to be smooth and well behaved. (The silver nitrate added to the reaction mixture to prevent spontaneous wave initiations was found to have a negligible effect on the front velocity.)

As the front develops from the boundary between the reactant and product zones, it initially has the geometry of the boundary itself. With a planar zone boundary and a cyclodextrin concentration less than about 0.12 M, the front propagates into the reactant zone retaining the planar symmetry. At higher cyclodextrin concentrations, however, the planar front loses its stability and develops a cellular structure. Figure 8 shows a cellular front in a reaction mixture with [cyclodextrin]$_0$=0.33 M. The structure resembles that of the front shown in Fig. 3, which was computed from Eqs. (5) and (10) with the same cyclodextrin concentration. Like the calculated front, the front in Fig. 8 is a snapshot of a continually changing structure. The cells are joined at minima which propagate as transverse waves. As in the calculated behavior, the velocity of these waves is much lower than the overall front velocity. The positions of the minima were measured at equal time increments and plotted as the front advanced into the reactant zone, as shown in Fig. 9. A comparison with the calculated behavior in Fig. 4 shows
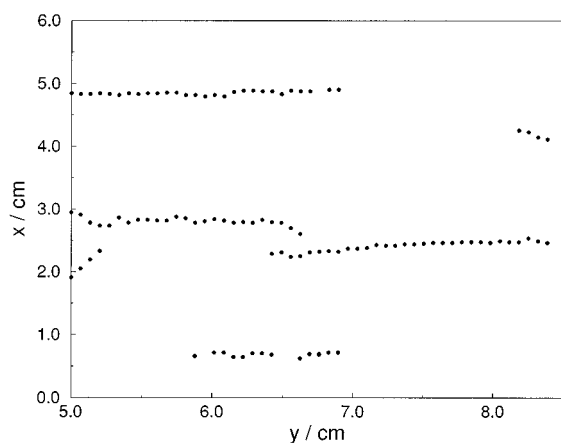

FIG. 10. Initial front evolution from a symmetrical perturbation with [cyclodextrin]$_0$=0.33 M. (a) Behavior at t=23 min following initiation at the interface between product and reactant zones. (b) Development of front at t=343 min after initiation showing appearance of a cusp separating two symmetrical cells.

similar trends, with the coalescence and spontaneous appearance of the minima.

Initial conditions with a symmetrical perturbation like that described in Sec. II B allow an examination of the initial evolution of the front. Experiments with a single, symmetrical perturbation were carried out with cyclodextrin concentration above and below the critical value. With [cyclodextrin]$_0$=0.33 M, the evolution of the front from the step perturbation shown in Fig. 10(a) occurs with a characteristic two-cell structure, as shown in Fig. 10(b). The structure is much like that of the front shown in Fig. 5(b), calculated from Eqs. (5) and (10) with the same cyclodextrin concentration. As the front propagates away from the product-reactant interface, the first sign of instability is the appearance of a small cusp in the center of the perturbed section. At longer times, several minima appear and the behavior becomes irregular like that observed with the planar initiation. Figure 11(b) shows the wave form when [cyclodextrin]$_0$=0.04 M, evolving from the initial perturbation shown in Fig. 11(a). The step perturbation is diffusively smoothed when the cyclodextrin concentration is below the critical value.

IV. DISCUSSION AND CONCLUSIONS

Instabilities in isothermal reaction-diffusion fronts arise from the decoupling of the activator and inhibitor species. In the iodate-arsenous acid reaction, the activator is the autocatalyst iodide and the inhibitor is the stoichiometrically limiting reactant iodate. The spatial decoupling arises from the formation of a complex between α-cyclodextrin and iodide,

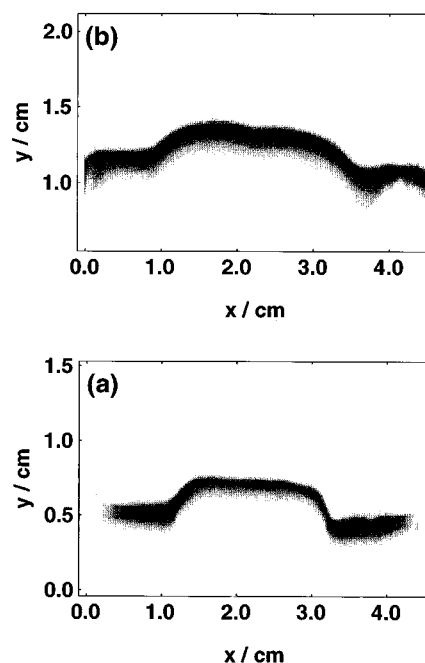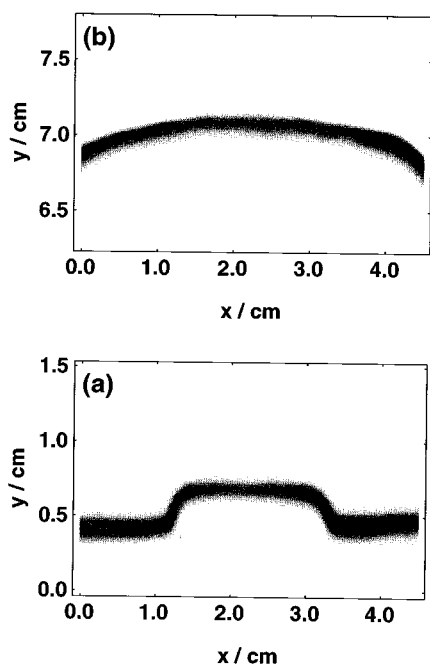

FIG. 9. Evolution of minima in the front shown in Fig. 8.

FIG. 11. Initial front evolution from a symmetrical perturbation with $[\text{cyclodextrin}]_0 = 0.04$ M. (a) Behavior at $t=23$ min following initiation at the interface between product and reactant zones. (b) Development of front at $t=10$ h after initiation showing the diffusive smoothing of the perturbation.

which is effectively immobilized in the gel medium. An additional requirement for the onset of instability in isothermal fronts is a cubic (or higher-order) nonlinearity in the rate law.[6,7] In mixed-order rate laws with both quadratic and cubic nonlinearities, the cubic channel must be dominant. This requirement is met by the iodate-arsenous acid reaction, where the quadratic channel comprises only a small fraction of the overall reaction.

Insights into the dependence of the front velocity on cyclodextrin concentration can be gained by considering limiting cases of the one-dimensional system. The complex formation has a double effect on the front velocity, with both the apparent diffusion coefficient of iodide as well as the apparent rate of iodide production decreasing with increasing cyclodextrin concentration. To explore these two effects, we assume that they are independent and examine them separately as limiting cases.

We first consider the case where only the rate of iodide production is lowered by a factor of σ with equal iodide and iodate diffusion coefficients. The system can now be described in terms of one variable, with the concentrations of iodide and iodate related by

$$[\text{I}^-] = \frac{[\text{IO}_3^-]_0 - [\text{IO}_3^-]}{\sigma}. \tag{11}$$

We follow an earlier treatment of quadratic and cubic mixed-order fronts,[7–9] which provides an analytical expression for the velocity. The one-variable system obtained by combining

Eqs. (10) and (11) is first transformed to a moving coordinate frame, with the new spatial variable $z = y' - vt'$.[21] This yields the ordinary differential equation

$$\frac{d^2\alpha}{dz^2} + v\frac{d\alpha}{dz} - \frac{\alpha(1-\alpha)^2}{\sigma^2} - \frac{\kappa\alpha(1-\alpha)}{\sigma} = 0, \tag{12}$$

where $\alpha = [\text{IO}_3^-]/[\text{IO}_3^-]_0$ and $\kappa = k_a/k_b[\text{IO}_3^-]_0$. This equation can be solved analytically by assuming a parabolic form for the gradient of α,

$$\frac{d\alpha}{dz} = C\alpha(1-\alpha), \tag{13}$$

where C is a constant to be determined. Combining Eqs. (12) and (13) and dividing by $\alpha(1-\alpha)$ yields the linear equation

$$C^2 + vC - \frac{1}{\sigma^2} - \frac{\kappa}{\sigma} = \left(2C^2 - \frac{1}{\sigma^2}\right)\alpha, \tag{14}$$

which can be solved for C and v:

$$C = 1/\sqrt{2}\,\sigma, \tag{15}$$

$$v = (1/\sqrt{2}\,\sigma) + \sqrt{2}\,\kappa. \tag{16}$$

Since $\kappa \ll 1$ for the iodate-arsenous acid reaction, the second term in Eq. (16) can be neglected. Thus, the front velocity decreases as $1/(2^{1/2}\sigma)$ with increasing cyclodextrin concentration due to the decrease in the apparent rate of iodide production.

For the opposite limit, where only the apparent diffusion coefficient of iodide decreases and its rate of production is unaffected, no analytical solution is available for the front velocity. However, Billingham and Needham[22] have shown that v is of $O(\sigma^{-1})$ when $\sigma \gg 1$ and of $O(\sigma^{-1/2})$ when $\sigma \ll 1$. These represent upper and lower limits for our case, where σ is of $O(1)$.

We define v_0 as the velocity of propagation when no cyclodextrin is present (i.e., $\sigma = 1$), and incorporate both effects to give an upper and lower bound for the velocity as a function of cyclodextrin concentration. Combining the limits $v \sim O(\sigma^{-1})$ for $\sigma \gg 1$ and $v \sim O(\sigma^{1/2})$ for $\sigma \ll 1$ with the first term of Eq. (16) yields

$$\frac{v_0}{\sigma^2} < v < \frac{v_0}{\sigma^{3/2}}. \tag{17}$$

These bounds are shown in Figs. 1 and 7 by the upper and lower dashed curves. Both the velocity dependence calculated from Eqs. (5) and (10) and the measured velocities fall between the upper and lower limits. This analysis relies on comparing velocities of the one-dimensional system with the measured and calculated velocities of the two-dimensional system. The two-dimensional calculations for $[\text{cyclodextrin}]_0 = 0.33$ M, such as in Fig. 2(b), yield a velocity that is about 3% higher than the one-dimensional calculations. There is no difference in velocity in the one- and two-dimensional calculations when $[\text{cyclodextrin}]_0 \lesssim 0.12$, suggesting that the lateral instability at higher concentrations facilitates the front propagation. The velocity difference at high cyclodextrin concentrations is negligible compared to the overall decrease in velocity caused by the complex formation.

The patterned fronts observed in the iodate-arsenous acid system are much like those found in our earlier study of instabilities in quadratic and cubic mixed-order fronts.[6] We have focused on the parameter range of the experiments in this investigation, where irregular behavior is observed in both the modeling calculations and the experiments. The qualitative appearance as well as the physical length scales of the patterned fronts are accurately predicted by the model. The agreement with the experimental behavior is remarkably good considering that no adjustable parameters were used. We note that the reduced diffusivities of both iodide and iodate in the highly cross-linked gel do not affect the critical diffusion coefficient ratio for the onset of instability.

Lateral instabilities in isothermal reaction-diffusion fronts and thermodiffusive instabilities in premixed flames share many common features. Cellular flames arise in reaction mixtures with a stoichiometrically deficient reactant having a high diffusivity. The cells are joined at cusps where the temperature is lower than along the foremost sections of the cells. Cellular flames exhibit extremely rich behavior, from stable structures to complex periodic rearrangements of cells to highly chaotic states where cells are annihilated and created.[23,24] Theoretical studies have revealed that thermodiffusive models are able to qualitatively reproduce much of the experimentally observed behavior, suggesting that hydrodynamic effects are of secondary importance in at least some cases of controlled combustion. Matkowsky and co-workers[25] have carried out extensive studies of the stable and oscillatory states of cellular flames. Transverse wave propagation is found in the periodic and chaotic states, much like the behavior of cellular reaction-diffusion fronts.[6]

The exponential dependence of reaction rate on temperature ensures the formation of thin fronts in flames. In the reaction-diffusion system, the weaker positive feedback of cubic autocatalysis gives rise to wider reaction fronts. This, in turn, results in smaller amplitude waves along the cellular front. Isothermal autocatalytic reactions with higher-order nonlinearities might give rise to more dramatic front instabilities like those observed in flames. Lateral instabilities also occur in pulse type waves of excitable media.[26,27] Such instabilities may play an important role in the recently discovered serpentine patterns of the FIS (ferrocyanide–iodate–sulfite) reaction.[28]

[1] J. D. Murray, *Mathematical Biology* (Springer-Verlag, Berlin, 1989).

[2] V. Castet, E. Dulos, J. Boissonade, and P. De Kepper, Phys. Rev. Lett. **64**, 2953 (1990).

[3] A. B. Rovinsky and M. Menzinger, Phys. Rev. Lett. **70**, 778 (1993).

[4] G. H. Markstein, J. Aeronaut. Sci. **3**, 18 (1951).

[5] G. I. Sivashinsky, Combust. Sci. Technol. **15**, 137 (1977).

[6] D. Horváth, V. Petrov, S. K. Scott, and K. Showalter, J. Chem. Phys. **98**, 6332 (1993).

[7] S. K. Scott and K. Showalter, J. Phys. Chem. **96**, 8702 (1992).

[8] A. Hanna, A. Saul, and K. Showalter, J. Am. Chem. Soc. **104**, 3838 (1982).

[9] A. Saul and K. Showalter, *Oscillations and Traveling Waves in Chemical Systems*, edited by R. J. Field and M. Burger (Wiley, New York, 1985), Chap. 11.

[10] P. De Kepper, I. R. Epstein, and K. Kustin, J. Am. Chem. Soc. **103**, 6121 (1981).

[11] S. Dushman, J. Phys. Chem. **8**, 453 (1904).

[12] J. Roebuck, J. Phys. Chem. **6**, 365 (1902).

[13] H. A. Liebhafsky and G. M. Roe, Int. J. Chem. Kinet. **11**, 693 (1979).

[14] N. Ganapathisubramanian and K. Showalter, J. Phys. Chem. **89**, 2118 (1985).

[15] H. Uedaira and H. Uedaira, J. Phys. Chem. **74**, 2211 (1970).

[16] J. F. Wojcik and R. P. Rohrbach, J. Phys. Chem. **79**, 2251 (1975).

[17] T. Sano, M. Yamamoto, H. Hori, and T. Yasunga, Bull. Chem. Soc. Jpn. **57**, 678 (1984).

[18] I. Lengyel and I. R. Epstein, Proc. Natl. Acad. Sci. USA **89**, 3977 (1992).

[19] Z. Noszticzius, W. Horsthemke, W. D. McCormick, H. L. Swinney, and W. Y. Tam, Nature **329**, 619 (1987).

[20] B. Neumann, Zs. Nagy-Ungvarai, and S. C. Müller, Chem. Phys. Lett. **211**, 36 (1993).

[21] See Ref. 6 for scaling: $y' = (k_b[\mathrm{H^+}]_0^2[\mathrm{IO_3^-}]_0^2/D)^{-1/2}y$ and $t' = (k_b[\mathrm{H^+}]_0^2[\mathrm{IO_3^-}]_0^2)t$.

[22] J. Billingham and D. J. Needham, Philos. Trans. R. Soc. London, Ser. A **334**, 1 (1991).

[23] M. el-Hamdi, M. Gorman, and K. A. Robbins, Combust. Sci. Tech. **94**, 87 (1993).

[24] M. Gorman, M. el-Hamdi, and K. A. Robbins, Combust. Sci. Tech. **98**, 25 (1994); **98**, 37 (1994); **98**, 47 (1994).

[25] A. Bayliss, B. J. Matkowsky, and H. Riecke, Physica D **74**, 1 (1994).

[26] J. E. Pearson, Science **261**, 189 (1993).

[27] V. Petrov, S. K. Scott, and K. Showalter, Philos. Trans. R. Soc. London, Ser. A **443**, 631 (1994).

[28] K. J. Lee, W. D. McCormick, Q. Ouyang, and H. L. Swinney, Science **261**, 192 (1993).